Journal of Structural Geology 31 (2009) 926–940

Contents lists available at ScienceDirect

Journal of Structural Geology

journal homepage: www.elsevier.com/locate/jsg

Growth trishear model and its application to the Gilbertown graben system, southwest Alabama

Guohai Jin [a,*], Richard H. Groshong, Jr. [a], Jack C. Pashin [b]

[a] Department of Geological Sciences, The University of Alabama, Tuscaloosa, AL 35487, USA
[b] Geological Survey of Alabama, P.O. Box 869999, Tuscaloosa, AL 35486, USA

ARTICLE INFO

Article history:
Received 29 March 2007
Received in revised form 1 April 2008
Accepted 16 September 2008
Available online 17 October 2008

Keywords:
Trishear modeling
Growth structures
Gilbertown graben system
Compaction
Structural geology

ABSTRACT

Fault-propagation folding associated with an upward propagating fault in the Gilbertown graben system is revealed by well-based 3-D subsurface mapping and dipmeter analysis. The fold is developed in the Selma chalk, which is an oil reservoir along the southern margin of the graben. Area-depth-strain analysis suggests that the Cretaceous strata were growth units, the Jurassic strata were pregrowth units, and the graben system is detached in the Louann Salt.

The growth trishear model has been applied in this paper to study the evolution and kinematics of extensional fault-propagation folding. Models indicate that the propagation to slip (p/s) ratio of the underlying fault plays an important role in governing the geometry of the resulting extensional fault-propagation fold. With a greater p/s ratio, the fold is more localized in the vicinity of the propagating fault. The extensional fault-propagation fold in the Gilbertown graben is modeled by both a compactional and a non-compactional growth trishear model. Both models predict a similar geometry of the extensional fault-propagation fold. The trishear model with compaction best predicts the fold geometry.

1. Introduction

Conventional normal faults are commonly listric (concave upward) in shape. The collapse of the hanging wall in response to extension in a listric normal fault is thought to be linked kinematically to the geometry of the fault (Gibbs, 1983; White et al., 1986; Williams and Vann, 1987; Groshong, 1990). The geometric relationship between a listric normal fault and its hanging wall deformation has been studied intensively during the past two decades (Dula, 1991; Schlische, 1995). A rollover anticline in the hanging wall is commonly observed associated with a listric normal fault.

The geometry of hanging wall deformation adjacent to a convex-upward normal fault is significantly different from that along a listric fault. A convex-upward fault may form during propagation of the growth fault from non-growth units to overlying growth units due to compaction (Roux, 1979; Xiao and Suppe, 1989). Experimental studies reveal that synthetic shear prevails immediately above a convex bend and that beds in hanging wall dip away from the master normal fault (Withjack et al., 1995). Xiao and Suppe (1992) concluded that the shear becomes synthetic at a convex fault bend, which allows the bed to thin across the bend rather than to thicken as required by antithetic shear (Groshong, 1996). However, the predicted geometry of hanging wall deformation from their kinematic model reveals kink-band style folding and may not be appropriate in interpreting the structures in the growth environment which commonly lack discrete dip domains (e.g., those discussed by Gawthorpe et al., 1997). So far, the kinematics of extensional fault-propagation folding associated with an upward convex fault are not well documented and are the subject of this study.

The Gilbertown graben system is located in Choctaw County, southwest Alabama (Fig. 1). Previous work in the area of the Gilbertown graben has focused on stratigraphy and sedimentation (Martin, 1978; Harris and Dodman, 1982; Tolson et al., 1983; Russell et al., 1983), regional structures and tectonics (Murray, 1961; Hughes, 1968; Martin, 1978; Worrall and Snelson, 1989; Pashin et al., 1998a, b; Groshong et al., 2003), subsurface mapping (Moore, 1971; Wilson et al., 1976), and production and reservoir analysis (Current, 1948; Braunstein, 1953; Bolin et al., 1989). Those works provide a wealth of knowledge of the geological history and the hydrocarbon production in the Gilbertown graben system. Recent structural studies (Pashin et al., 1998a, b, 2000) indicated that the major graben-bounding faults usually dip about 60° in the Jurassic and Early Cretaceous units and flatten in the Selma Group and the subsequent younger units, indicating they are convex-upward. 3-D subsurface mapping and dipmeter analysis

* Corresponding author. Geological Survey of Alabama, P.O. Box 869999, Tuscaloosa, AL 35486, USA.
E-mail address: gjin@gsa.state.al.us (G. Jin).

0191-8141/$ – see front matter © 2008 Elsevier Ltd. All rights reserved.
doi:10.1016/j.jsg.2008.09.006

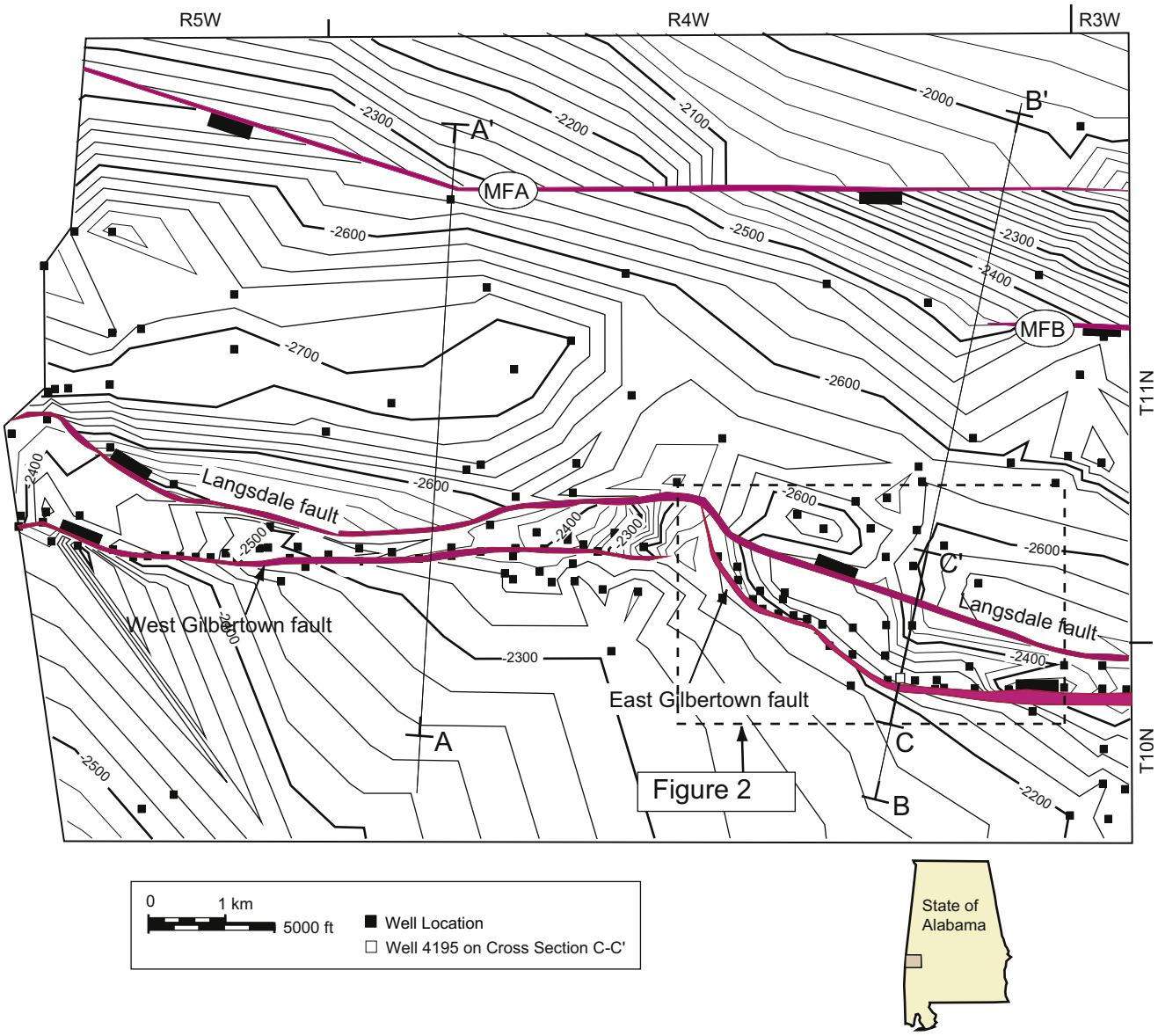

Fig. 1. Structure contour map of the top Selma Group in the Gilbertown graben. MFA = Melvin fault branch A, MFB = Melvin fault branch B. Contours are below sea-level with 20 ft interval. A–A′, B–B′, and C–C′ are cross sections in Figs. 4–6, respectively.

(Pashin et al., 1998b; Jin et al., 1999) shows that structure in the Gilbertown graben system at the level of the Cretaceous Selma Group is an extensional fault-propagation fold in the hanging wall of the graben-bounding fault.

The trishear model is a distributed shearing model and has been used successfully in modeling fault-related folding with remarkable success. While the model has been used to predict growth and pregrowth structures in a contractional setting (Hardy and Ford, 1997; Allmendinger, 1998), its application to an extensional setting is, so far, limited to non-growth structures (Hardy and McClay, 1999). In this paper, we use the trishear model to elucidate the extensional fault-propagation folding mechanism of the Gilbertown graben system, which includes an upward convex syndepositional fault. The convex shape of the graben-bounding fault is modeled by differential compaction. To accomplish this, we first use the trishear model to examine the relationships between the deformation of the growth structure associated with an underlying propagating extensional fault and the different modeling parameters. We then apply the growth trishear model with appropriate parameters to a cross section in the eastern Gilbertown graben system (Fig. 2) to evaluate the applicability of the model.

2. Geological setting

The Gilbertown graben system strikes east–west, is bounded by the Gilbertown and Melvin fault systems, and is 5–8 km wide and 35 km long at the surface. The Gilbertown fault system is subdivided into the Langsdale fault (Fig. 1), the West Gilbertown fault, and the East Gilbertown fault. The Melvin fault system is composed of Melvin faults A and B, which are linked by a relay ramp. The Gilbertown graben system is a nearly symmetrical graben detached in the Jurassic Louann Salt at the updip limit of salt in the Gulf of Mexico basin; it is part of the peripheral fault trend of the Gulf Coast basin. Structural restorations indicate that the Gilbertown graben system began forming as a half graben during Early Cretaceous time and became a full graben during the Late Cretaceous (Pashin et al., 1998a, b, 2000).

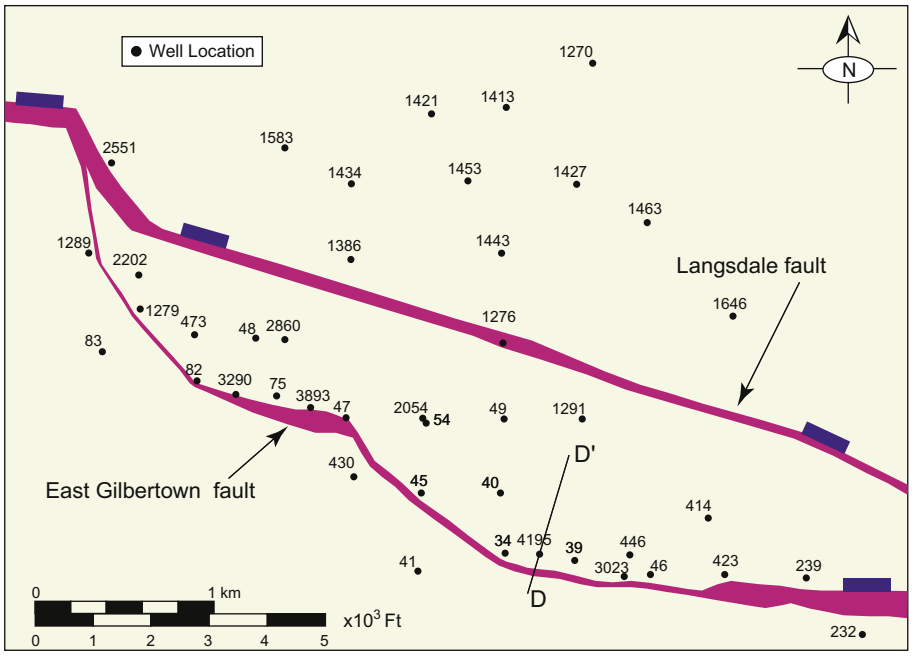

Fig. 2. Map view of focus area. See Fig. 1 for location. Numbers associated with well locations are Alabama state permit numbers. The width of the faults indicates the amount of stratigraphic separation at the level of top Selma Group. The cross section D–D′ is used for trishear kinematic modeling in this paper.

Considerable structural growth in the Cretaceous section of the Gilbertown graben system has been recognized by previous workers (Current, 1948; Wilson et al., 1976; Pashin et al., 1998b). Isopach maps for different stratigraphic units indicate that sediment thickness of each unit in the graben is usually 20–30% thicker than its equivalent outside the graben (Pashin et al., 1998a). Vertical separation of the top of the Eutaw Formation across the Gilbertown fault system is approximately 400 ft. Displacement increases with depth; and, along parts of the fault systems, the vertical separation of the Smackover Formation exceeds 1500 ft (Wilson et al., 1976; Pashin et al., 1998a, b). The Jurassic strata and the Cotton Valley Group can be treated as effective pregrowth stratigraphy. Most structural growth took place during the Early Cretaceous.

The convex-upward geometry of the graben-bounding faults has been revealed by cross section construction and balancing (Pashin et al., 1998a) and is further confirmed by detailed 3-D subsurface mapping from well log data (Jin et al., 1998) and 3-D fault curvature models (Pashin et al., 2000). Graben-bounding faults in individual wells are recognized from resistivity logs where a high-resistivity zone normally 10–50 ft in thickness occurs (Pashin et al., 1998). The stratigraphic separation for each fault cut is determined from the spontaneous potential (SP) logs by the amount of missing stratigraphy. Correlation of the graben-bounding faults indicates that faults generally dip 60° below the Selma Group. Within the Selma Group and younger units, those faults dip as gently as 45°.

Cross section balancing (Pashin et al., 1998b) and dipmeter analysis (Jin et al., 1998; Pashin et al., 1998b, 2000) provide evidence for extensional fault-propagation folding in the Gilbertown graben system. Pashin et al. (1998b) used the area-depth method (Epard and Groshong, 1993; Groshong, 1994) and found that the negative requisite strain in the growth units (e.g., the Selma Group) can be made positive or zero by including an extensional fault-propagation fold in the hanging wall adjacent to the graben-bounding fault. Dipmeter logs indicate that dip in the footwall is minimal, and the dip sequence in the hanging wall indicates that Selma chalk is deformed into an extensional fault-propagation fold immediately adjacent to the graben-bounding fault (Jin et al., 1998). Although the geometry of the extensional fault-propagation fold in the Selma Group may not be detectable from subsurface mapping using well-log correlation alone, it is of great importance in controlling fracturing and, hence, the hydrocarbon production from Selma chalk (Pashin et al., 1998b, 2000).

3. Detailed extensional fault-propagation geometry in the Gilbertown graben system

The detailed geometry of the extensional fault-propagation fold is derived from a complete 3-D interpretation of the structure. The fault cuts and stratigraphic markers for each well were picked from SP and resistivity logs. The vertical separation of each fault was determined from the amount of missing section from SP logs. Faults were correlated in adjacent wells from fault cuts with similar amounts of stratigraphic separation. For growth faults, the vertical separation increases downward. Cross sections were produced by slicing the 3-D model.

Cross section balancing using the area-depth technique proposed by Epard and Groshong (1993) was applied to two cross sections from the 3-D structural model in order to evaluate the accuracy of the interpretation of the graben structure. Figs. 3a and 4a are two cross sections constructed from the east and west portions of the 3-D model, respectively, and are nearly perpendicular to the graben-bounding faults. The regionals (stratigraphic boundaries not involved in deformation) of the stratigraphic units in the south side of the graben in both cross sections are systematically lower than those in the north side of the graben, especially for these deep units. This is the result of subsidence of the southern block caused by the withdrawal of the Louann Salt during the evolution of the graben. The downward shift of the regionals has no effect on lost area estimation in units above the salt as long as the southern regionals are used (Qi et al., 1998; Groshong et al., 2003).

The area-depth curves measured from the two cross sections indicate that they are internally consistent. The area-depth curves

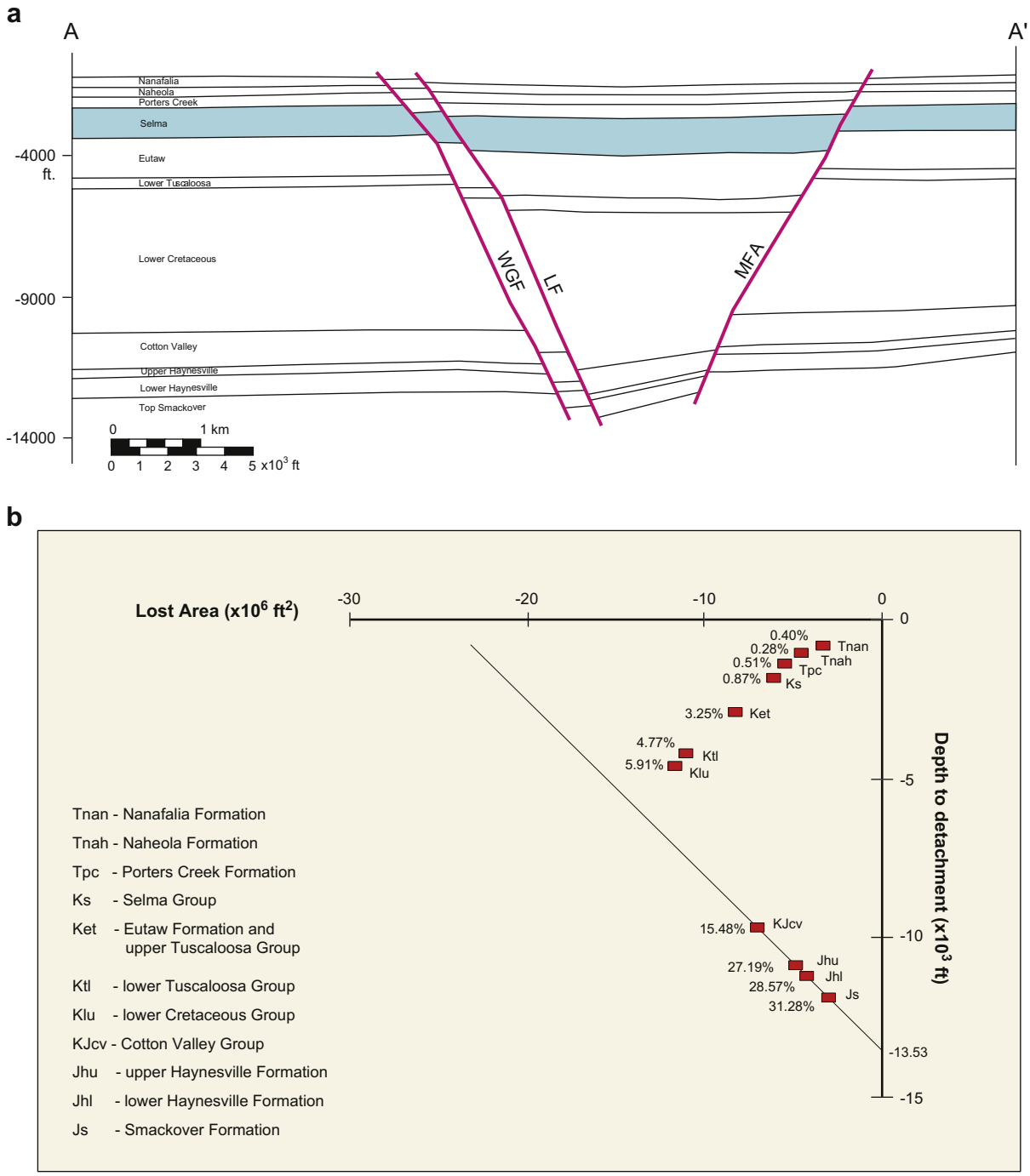

Fig. 3. Cross section A–A′ cutting from the 3-D model and the corresponding area-depth plot in the Gilbertown graben system. WGF = West Gilbertown fault, MFA = Melvin fault A. No vertical exaggeration. For location see Fig. 1.

for the lowest four units are straight lines (Figs. 3b and 4b). Since the slope of the regression line is the inverse displacement (Groshong, 1994), it suggests that displacement is constant for all units belonging to the pregrowth sequence. The depth to the detachment predicted by the least-squares lines (Figs. 3b and 4b) is approximately 13,500 ft below sea level, coinciding with the top of the Louann Salt, which is presumably the basal detachment (Pashin et al., 1998b). In the Cretaceous units, the area-depth relationship follows a trend with progressively smaller lost area in the younger units, indicating that displacement of the successive units decreases upward because of syndepositonal growth (Qi et al., 1998; Groshong et al., 2003). The large and positive requisite strains in the pregrowth beds (Smackover-Cotton Valley) are not surprising in a full graben because they are close to the predicted detachment where large strains commonly occur to accommodate the deformation in response to extension (Groshong, 1994). The small requisite strains in the upper Cretaceous section suggest that the graben-scale internal deformation within those units is not significant.

The geometry of the extensional fault-propagation fold has been examined in detail for an area in the eastern part of Gilbertown field (Fig. 2). Fig. 5a is a transverse dip component

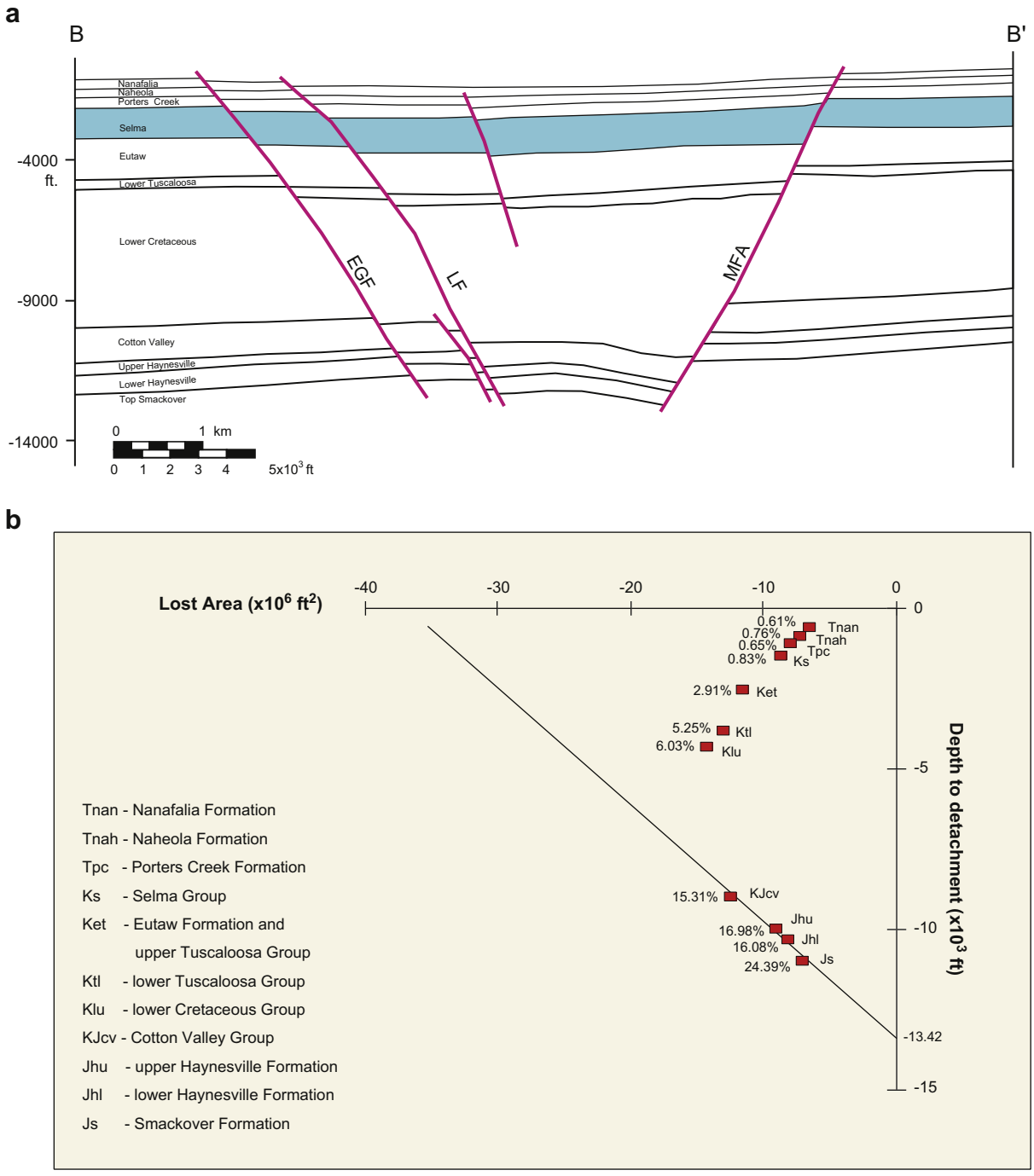

Fig. 4. Cross section B–B′ cutting from the 3-D model and the corresponding area-depth plot in the Gilbertown graben system. EGF = East Gilbertown fault, MFB = Melvin fault B. No vertical exaggeration. For location see Fig. 1.

versus depth plot (T-component plot) of dipmeter readings from well 4195 in the Selma chalk. Based on Bengtson (1981), each cusp marks the location of a fault. Seven distinctive cusps are identified that represent seven fault cuts, namely faults A through G. The interpreted geometry of the extensional fault-propagation fold is illustrated in Fig. 5b with the averaged dips in the transverse direction shown. Correlation to the nearby wells using SP logs indicates that fault G (at −2833 ft) is the East Gilbertown fault, which has a stratigraphic separation of about 100 ft. The stratigraphic separation of fault D (at −2488 ft) is about 75 ft. Fault G is interpreted to be the Gilbertown fault, and fault D is a splay of fault G. Together, the total separation is similar to that in other wells penetrating this fault (Fig. 5b). Other faults are thought to be the secondary faults within the extensional fault-propagation fold (Fig. 5b).

Fig. 5 further reveals a special feature of the fold geometry. Dip below fault G is close to zero, and the azimuth is randomly distributed, indicating that the fold is confined mainly to the hanging wall. The footwall is nearly flat and not involved in the fault-related deformation. The steepest dips are located in the hanging wall close to the fault and can be up to 40° (Fig. 5a). In the hanging wall, dip progressively decreases with distance from

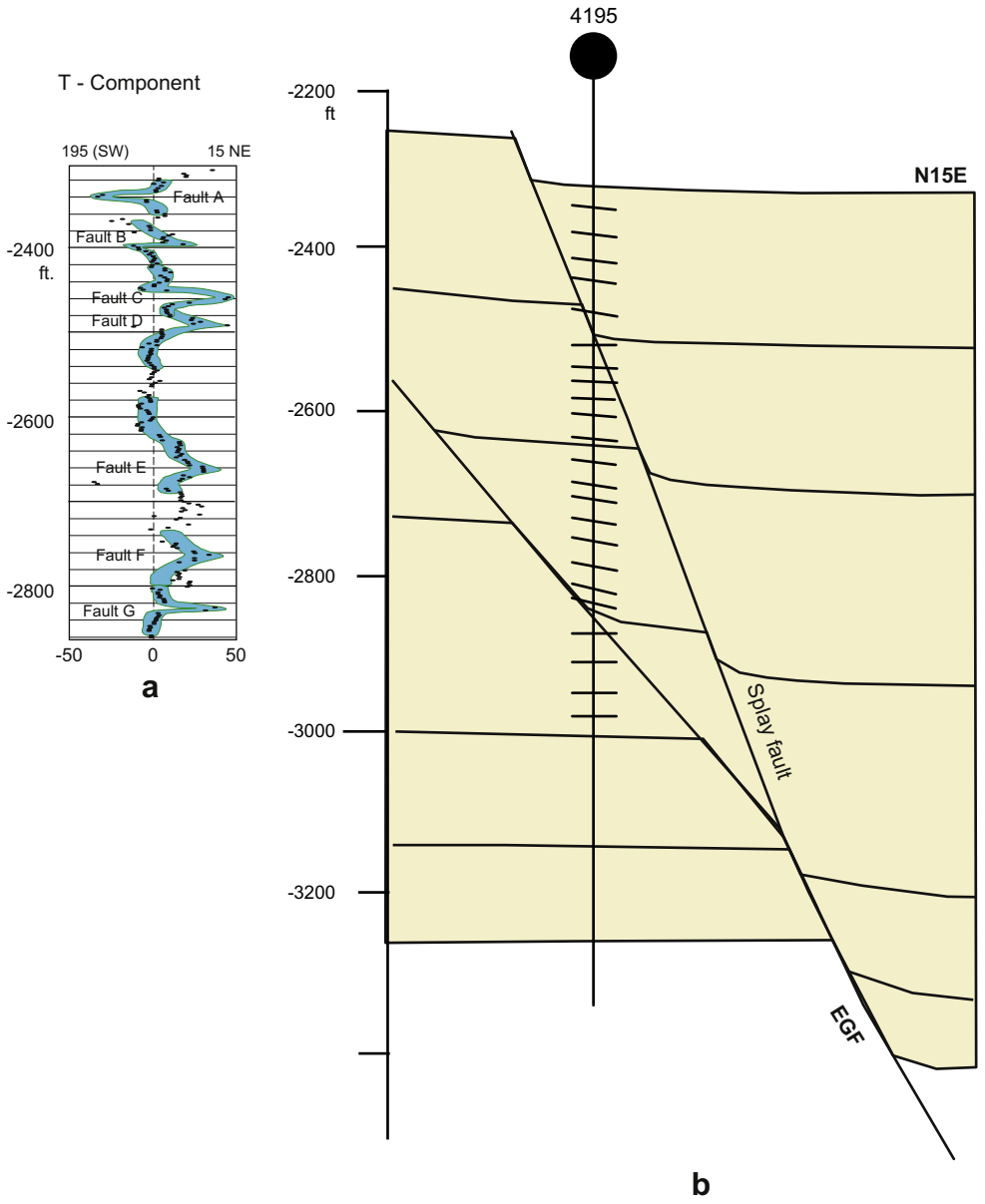

Fig. 5. Geometry of extensional fault-propagation fold shown by dipmeter log in well 4195. (a) Transverse dips versus depth plot indicating the locations of East Gilbertown fault (EGF), the splay fault, and other secondary faults. (b) Extensional fault-propagation fold interpreted from the apparent dips (short lines along well 4195) perpendicular to EGF.

the fault. An upward widening triangular zone of extensional fault-propagation within the Selma chalk is defined based on the dipmeter log (Fig. 5). Outside the fold zone, the dip of bedding returns to the regional dip.

Because our primary interest in extensional fault-propagation folding is within the Selma Group, a refined 3-D geometric model has been constructed for the East Gilbertown fault system (Fig. 2). The refined model is composed of the Eutaw Formation, Selma Group, Porters Creek Formation, Naheola Formation, and the Nanafalia Formation. The Selma Group has been subdivided into eight stratigraphic units labeled S_1 through S_8 as defined by Pashin et al. (1998a). These units can be identified from SP and resistivity logs and can be correlated with confidence throughout the mapped area (Fig. 6). Unit S1 overlies the Eutaw Sandstone and is distinguished by higher resistivity than other parts of the Selma Group. The other intervals can be identified by changes in the SP log. Fig. 6 shows the correlation of those eight units within the Selma Group from SP and resistivity logs in some sample wells located in different structural units in the focus area shown in Fig. 2.

Fig. 7 shows the cross section C–C′ which was sliced from the refined 3-D model. All subunits of the Selma Group are also shown in the figure except for S_2 and S_6 from the dipmeter log described earlier. This cross section serves as a template for the fold structure to be modeled kinematically.

4. Growth trishear deformation

Because growth beds commonly indicate the kinematic history of rock deformation (Allmendinger, 1998) and there is no previous paper dealing with the growth trishear modeling on extensional structures, we apply the trishear model (Erslev, 1991; Zehnder and Allmendinger, 2000; Jin and Groshong, 2006) to ideal examples of growth extensional fault-propagation folding. The basic properties

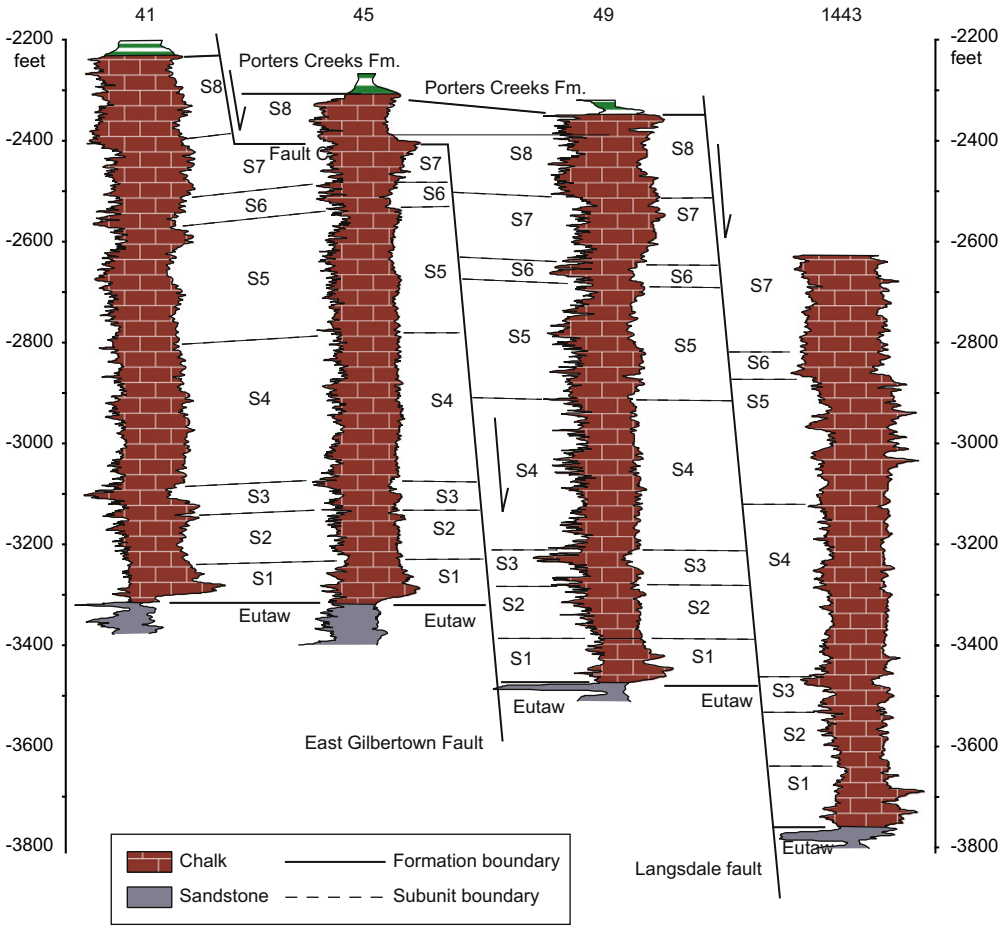

Fig. 6. Correlated well logs of the Selma Group showing internal stratigraphy and characteristics of East Gilbertown and Langsdale faults. For each well, the SP log is displayed on the left and resistivity log on the right. S_1 through S_8 are subunits within the Selma Group and are identical to those defined by Pashin et al. (1998a).

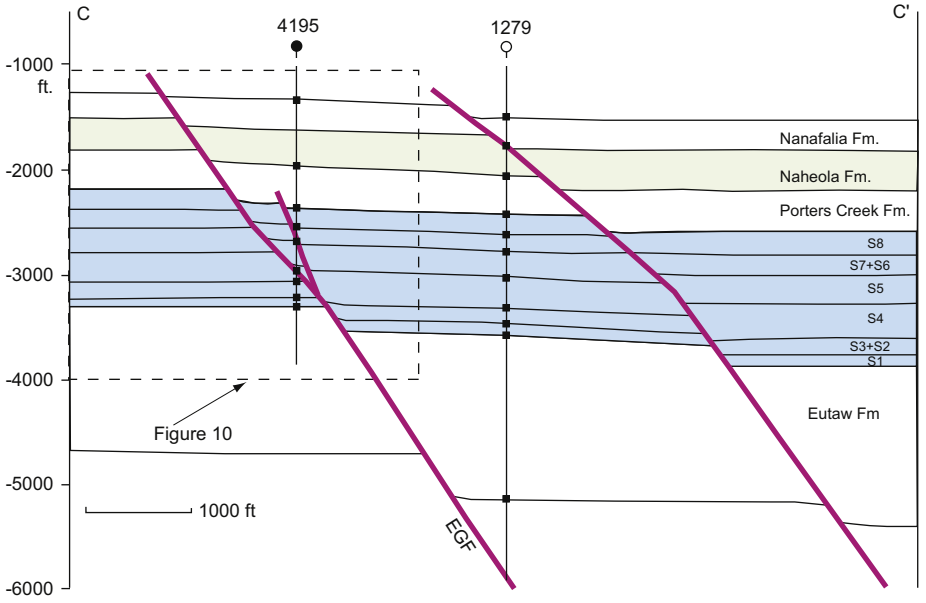

Fig. 7. Cross section C–C′ (see Fig. 1 for location). S1–S7 are units within the Selma Group. Wells are identified by Alabama Oil and Gas Board permit numbers. EGF = East Gilbertown fault. No vertical exaggeration.

of growth trishear deformation are investigated to better understand the general features associated with the resulting structures. Although the geometry of a growth structure can be related to a number of factors such as the rate of fault-propagation, the rate of deposition of new sediment and the mechanics of rocks involved in deformation both in pregrowth and growth strata, we focus our discussion on the influence of p/s ratios. The p/s ratio measures the magnitude of fault-tip propagates (p) relative to the slip(s) of the fault.

Figs. 8 and 9 show models run with four different p/s ratios. The models are composed of three different units. A precut pregrowth unit is at the bottom of the model, overlain by an initially unfaulted pregrowth unit (shaded), and then the growth unit, which is deposited during the deformation. At the initial stage, only the lower two units exist, and there is no growth unit. As soon as displacement starts, the growth layers are deposited at a rate that is the same as the vertical slip rate. In all four models, the dip of the fault is 60°, the apical angle is 70°, the velocity field factor r which governs the velocity field within the trishear zone (Jin and Groshong, 2006), and the total slip along the fault are the same. The only variable parameter is the p/s ratio, namely 0.0, 1.0, 2.0 and 4.0 for Figs. 8a,b and 9a,b, respectively.

Deformation of the initially unfaulted pregrowth units and in the growth units is characterized by progressive steepening of bedding. While deformation is continuing, the older growth units experience more downward movement than younger units. This causes the older beds in the growth units to dip more steeply than the younger units. Bedding is horizontal in the most recently deposited unit. This is a commonly observed feature of growth strata (e.g., Anadon et al., 1986; Suppe et al., 1992).

The growth beds in an extensional fault-propagation fold can be clearly distinguished from the pregrowth beds through the geometry of the growth triangle. A growth triangle is bounded by new trishear boundaries called active growth trishear boundaries in both the hanging wall and the footwall. While the displacement along the underlying fault progresses and new beds are deposited, the growth beds progressively steepen downward. At the same time, the separation between the active trishear boundary and the inactive trishear boundary in the hanging wall becomes greater, because the inactive trishear boundary remains fixed in the hanging wall while the active trishear boundary is fixed at the moving fault tip. A sharp bend is observed from the inactive trishear boundary to the active growth trishear boundary in the hanging walls (Figs. 8 and 9) and in the footwalls where the p/s ratio is greater than zero (Figs. 8b and 9). The location of the bend is the horizon where the growth begins.

The p/s ratio is an important control on the geometry of the fault-propagation fold in the growth strata. When p/s is zero, the active growth trishear boundary diverges upward from the trend of the fault line in both the hanging wall and the footwall (Fig. 8a). When the p/s ratio is 1.0, the fault-propagates at a rate the same as the deposition rate of the growth strata and thus the distance between the fault tip and the top of the depositional surface is always the same in this model (Fig. 8b). Therefore, the active growth trishear boundary is parallel to the fault line. If the p/s ratio increases to 2.0, the fault-propagation rate is two times the depositional rate and thus results in an active growth trishear boundary that converges upward toward the fault tip line. When the p/s ratio is 4.0, the geometry of the extensional fault-propagation fold is similar to that in Fig. 9a except that it pinches out

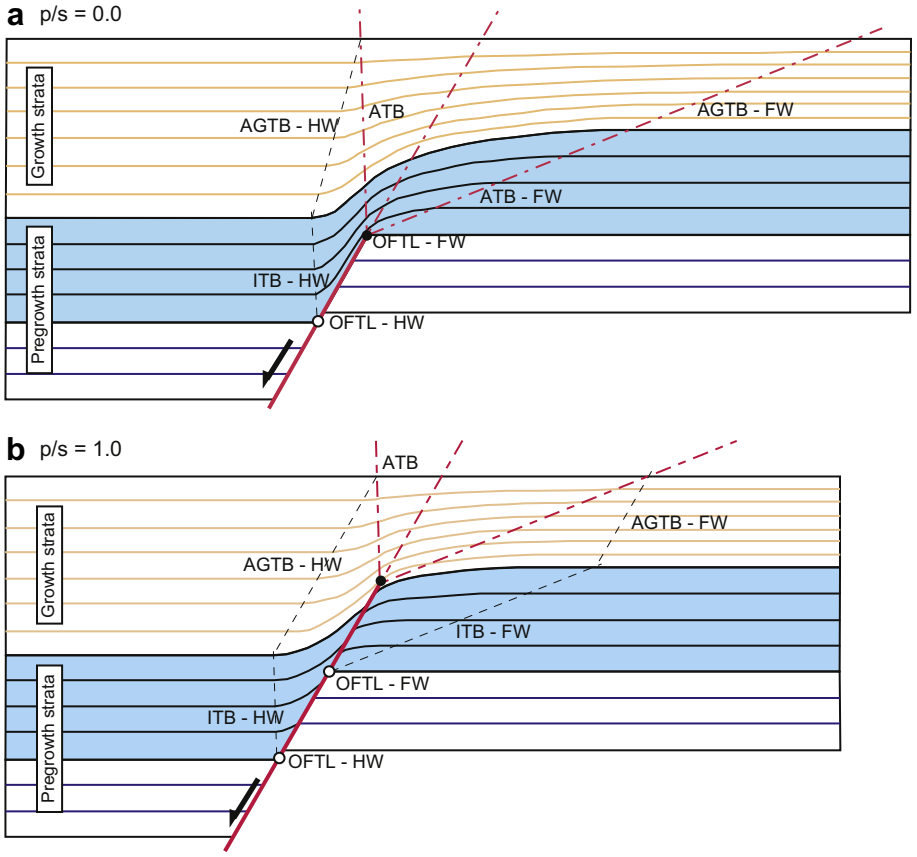

Fig. 8. Growth extensional fault-propagation folds predicted with the trishear model with p/s ratios 0.0 (a) and 1.0 (b). In both cases, $r = 0.8$, apical angle = 70°, the growth rate is equal to vertical component of the slip rate. HW = hanging wall, FW = footwall, OFTL = Original fault tip location, ATB = active trishear boundary, ITB = inactive trishear boundary, AGTB = active growth trishear boundary.

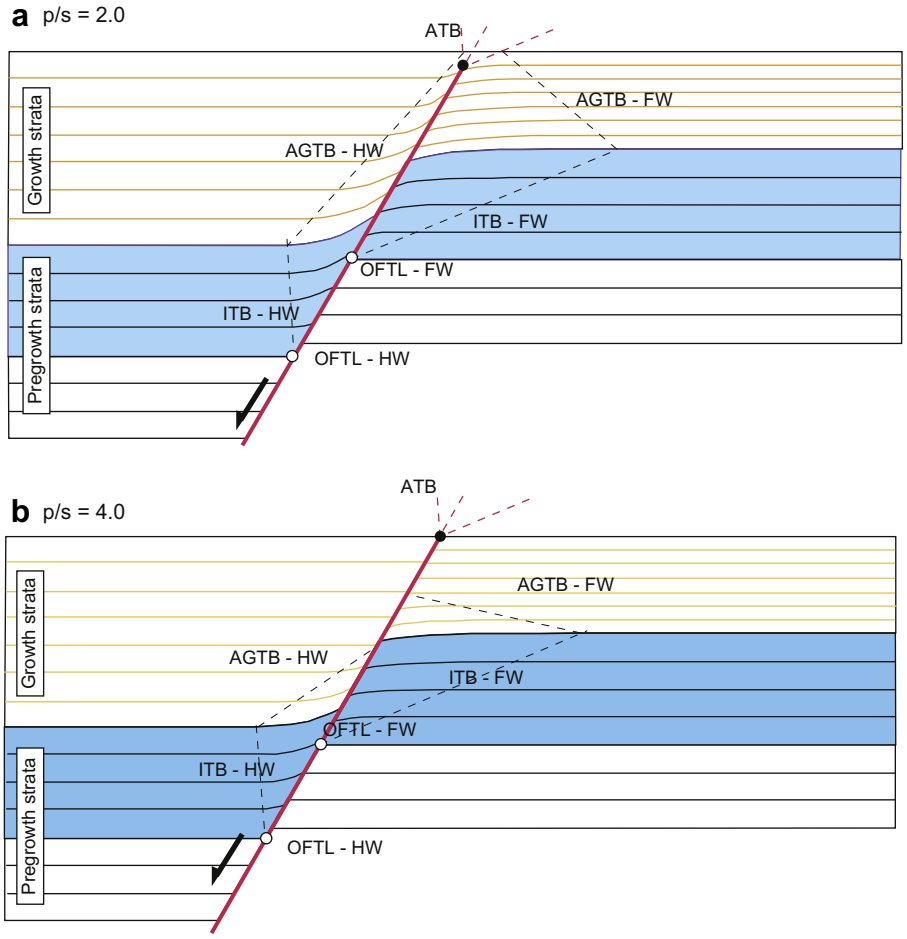

Fig. 9. Growth extensional extensional fault-propagation folds predicted with the trishear model with *p*/*s* ratios 2.0 (a) and 4.0 (b). In both cases, $r = 0.8$, apical angle = 70°, the growth rate is equal to vertical component of the slip rate. HW = hanging wall, FW = footwall, OFTL = original fault tip location, ATB = active trishear boundary, ITB = inactive trishear boundary, AGTB = active growth trishear boundary.

quickly in the younger growth units (Fig. 9b). This is because the fault-propagates upward so quickly that it reaches the top of the depositional surface shortly after deformation begins. Deformation of the growth strata thereafter is by rigid block translation along the fault.

5. Growth trishear modeling of the Gilbertown graben

A cross section illustrating the extensional fault-propagation fold geometry in Gilbertown field (Fig. 10) is the template for the growth trishear model. The extensional fault-propagation fold is developed primarily within the Selma chalk. The subunits of the Selma were used to characterize the fold geometry and were modeled sequentially by the trishear model. Modeling of the extensional fault-propagation fold included two growth trishear models, one without compaction and one with compaction, and a compaction alone model.

5.1. Compaction alone model

Compaction is an important factor in diagenesis (Athy, 1930; Dickinson, 1953; Perrier and Quiblier, 1974; Hamilton, 1976; Roux, 1979; Wilson and McBride, 1988; Houseknecht, 1987; Gay, 1989; Cowie and Karner, 1990). In a growth environment, early compaction is generally the most significant component of diagenesis (O'Connor and Gretener, 1974; Baldwin and Butler, 1985). Differential compaction structures result from lateral differences in compaction caused by changes in lithology, diagenesis, or thickness (Labute and Gretener, 1969; Billingsley, 1982; Davison, 1987). For a faulted structure, if the hanging wall compacts the most, a hanging wall syncline is produced; if the footwall compacts the most, a rollover into the fault is produced (Roux, 1979; Skuce, 1996).

Mechanical compaction is the most important compaction process for chalk at burial depths up to 3500 ft (Scholle, 1977). During the early stage of burial, mechanical compaction of chalk accounts for significant porosity reduction, and the amount of compaction can be well predicted using the empirical porosity-depth relationship (Hancock and Scholle, 1975; Scholle, 1977). At burial depths greater than 3500 ft, chalk no longer progresses along the typical compaction curve, which indicates that other processes, such as overpressuring, pressure solution, or chemical cementation, control the diagenesis. In the Gulf Coast chalk units, such as the Selma and Austin Groups, mechanical compaction is the most important process responsible for the loss of porosity (Scholle, 1977).

Modeling of extensional fault-propagation folding in the Gilbertown graben system with compaction requires using the original uncompacted thickness obtained from the present thickness. In the Gilbertown area, direct measurements of the porosity of the Selma chalk are not available. Thus the chalk porosity is calculated from the well log data. We used the sonic logs available from the

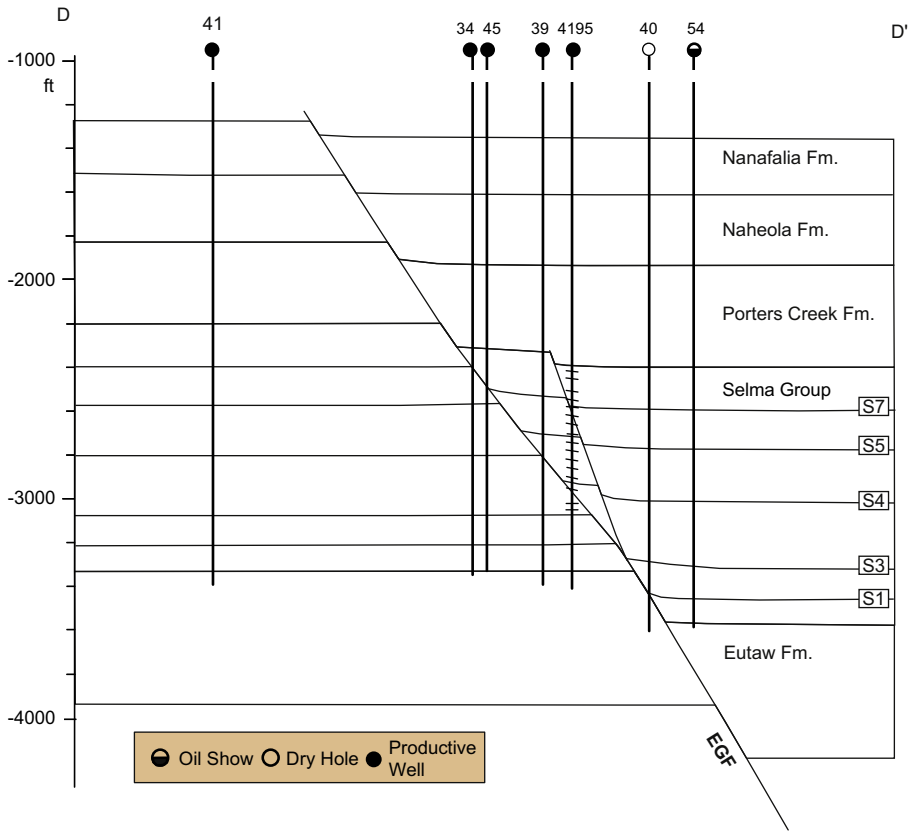

Fig. 10. Cross section D–D′ illustrating the geometry of the extensional fault-propagation fold on the East Gilbertown fault (EGF). See Fig. 2 for location. The bedding in well 4195 is interpreted from a dipmeter log. Nearby wells are projected onto the cross section so as to maintain their perpendicular distance to the EGF at the top of the Selma Group.

study area to calculate the porosity of the chalk following the method of Schlumberger (1989) and used the averaged porosity for each subunit. The porosity is used for decompaction to predict original thickness using the following equation (Xiao and Suppe, 1989):

$$\frac{h_0}{h_1} = \frac{\tan(1-\phi_1)}{\tan(1-\phi_0)}$$

where h_0 and h_1 are the original and compacted thickness for each bed and ϕ_0 and ϕ_1 are the original and compacted porosity, respectively. Table 1 shows the porosity and thickness of Selma chalk before and after compaction. The original porosity of Selma chalk is assumed to be 60% (Scholle, 1977).

Sequential modeling of the extensional fault-propagation fold using compaction alone for cross section D–D′ is shown in Fig. 11. In this model, the growth rate of the fault is the same as the depositional rate of the syndeformation sequences. Therefore, the tip of the fault is always located at the depositional surface. The dip of the fault is always 60°, and the dip change is completely determined by the amount of compaction of the Selma Group. No trishear deformation is considered in this model.

Table 1
The porosity and thickness for the Selma chalk before and after compaction

Subunit	Present thickness (ft)	Original thickness (ft)	Original porosity (%)	Present porosity (%)
S8	220.00	340.92	60.0	42.0
S7	160.00	253.38	60.0	41.0
S6	40.00	63.35	60.0	41.0
S5	260.00	429.81	60.0	39.0
S4	310.00	523.45	60.0	38.0
S3	70.00	120.72	60.0	37.0
S2	110.00	189.70	60.0	37.0
S1	120.00	211.32	60.0	36.0

The resulting geometry of this model reveals some characteristic features. First, there is no bedding dip in either the hanging wall or footwall in the vicinity of the growth fault where the same lithology is juxtaposed against the fault. This is because rocks from both sides of the fault underwent the same amount of compaction at the same burial depth. Second, a narrow zone of bedding dip is developed in the hanging wall right above the fault where the Selma Group is juxtaposed against the Eutaw Formation. This zone of compaction-related dip is bounded by two vertical dashed lines in Fig. 11. Because compaction is equivalent to vertical simple shear, differential compaction between the Selma chalk and the Eutaw sandstone creates the bedding dip in the Selma chalk in the hanging wall. Outside this zone, there is no compaction-induced bedding dip. The only change in this area is the thickness of beds. The predicted geometry does not match well to the extensional fault-propagation fold shown in Fig. 10. Therefore, it is concluded that compaction alone cannot satisfactorily explain the origin of the extensional fault-propagation fold in the Gilbertown graben system.

5.2. Extensional fault-propagation fold without compaction

No compaction is considered in this model. The change of fault dip in the cross section is modeled by changing directions of

fault-propagation in the trishear model. Based on the cross section, the initial hanging wall apical angle is about 35°. Because there is no hard evidence to determine whether the footwall is deformed, the initial footwall trishear apical angle was set to be 25° after a number of trial-and-error tests, which defines the the total trishear angle as 60° and $r = 0.8$.

Sequential evolution of the extensional fault-propagation folding is modeled by the growth trishear model and is shown in Fig. 12. The initial stage shows that the Eutaw Formation is cut by a fault with 60° dip (Fig. 12a). Unit S_1 was deposited on the top of the Eutaw Formation and was not initially faulted. The initial p/s ratio for the Eutaw Formation is 6.0. The fault keeps propagating at this rate into S_5 with a smaller dip of 52° until a splay fault is initiated (Fig. 12c,d). The splay fault is modeled as a fault without propagation after deposition of the Selma units because there is no evidence that displacement along this splay fault causes additional curvature of bedding (Fig. 12e). Thus, the deformation associated with the splay fault is simple rigid-body translation.

The original fault-propagates with a progressively higher p/s ratio after deposition of the Selma Group with a steeper dip of 55° (Fig. 12f,g). The actual p/s ratios in the later stage of deformation are 12.0, 20.0, and 40.0 during deposition of the Porters Creek Formation, the Naheola Formation, and the Nanafalia Formation, respectively. The progressively higher p/s ratios result in less trishear-induced bending of bedding within three younger

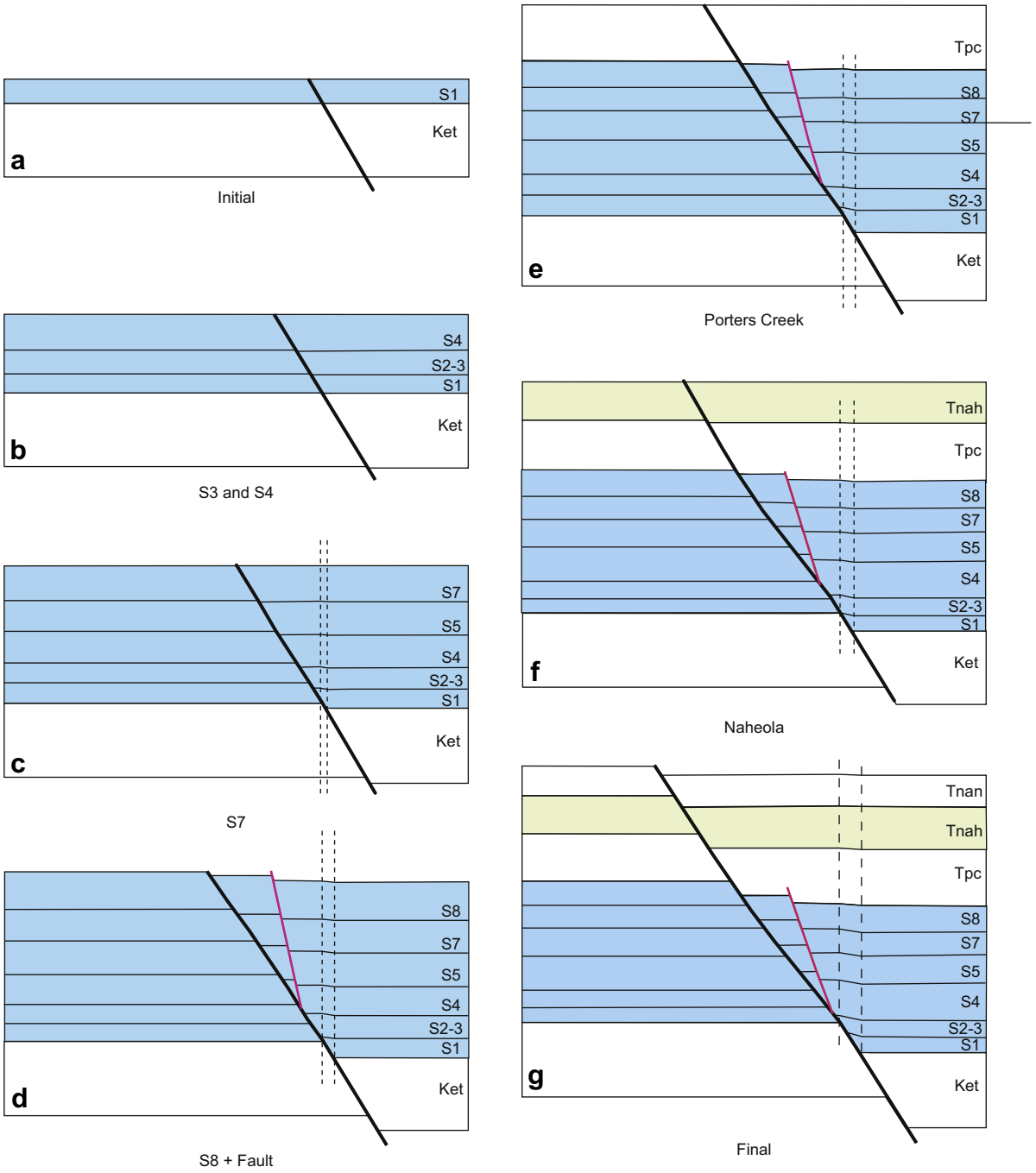

Fig. 11. Sequential forward modeling for cross section D–D′ using compaction only model. The dip of the fault is controlled by the amount of compaction. Two vertical dashed lines mark the boundary of the zone of dip caused by differential compaction.

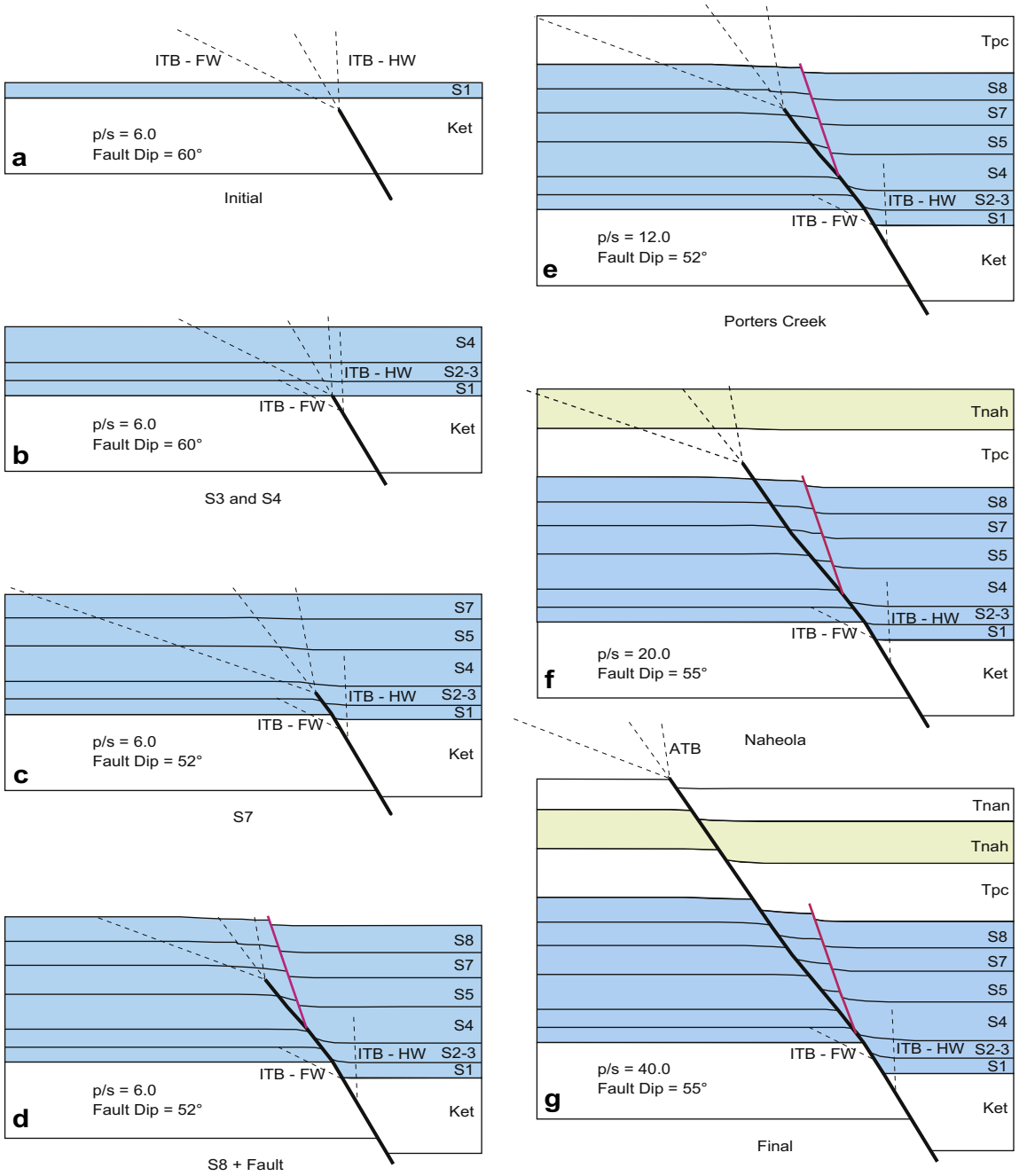

Fig. 12. Sequential forward modeling of cross section D–D′ (Fig. 10) using a trishear model. The fault is initially created in the Eutaw Formation and propagates upsection as successive beds are deposited. The *p*/*s* ratios and fault dips are changed during propagation. ATB = active trishear boundary, ITB–HW = inactive trishear boundary in hanging wall, ITB–FW = inactive trishear boundary in footwall.

units, which is required to fit the geometry of the cross section (Fig. 10).

The geometry of the fold in the cross section is fairly well predicted by this model. Because the *p*/*s* ratios are large, folding is localized in the hanging wall, especially in the younger units (Fig. 12). In the footwall, the width of the zone involved in the deformation is significantly larger than that in the hanging wall and the curvature of bedding is much less. A small mismatch between the predicted trishear geometry and the actual fold geometry occurs in the footwall close to the fault, where the model predicts slightly more folding than is observed. Including compaction in the model, as done in the next section, improves the fit.

The strain distribution associated with the trishear fold is predicted in Fig. 13. The greatest strain occurs where bedding has the greatest curvature. The strain ellipses also indicate that the distributed strains are localized along the propagating fault. In the footwall, the strain ellipses predicted by the trishear model show very little deformation.

5.3. Extensional fault-propagation fold with compaction

Because compaction in the Selma chalk causes significant change of fault dip and the bed thickness as indicated by the previous compaction alone model, the compaction process is modeled together with the growth trishear model. Fig. 14 shows

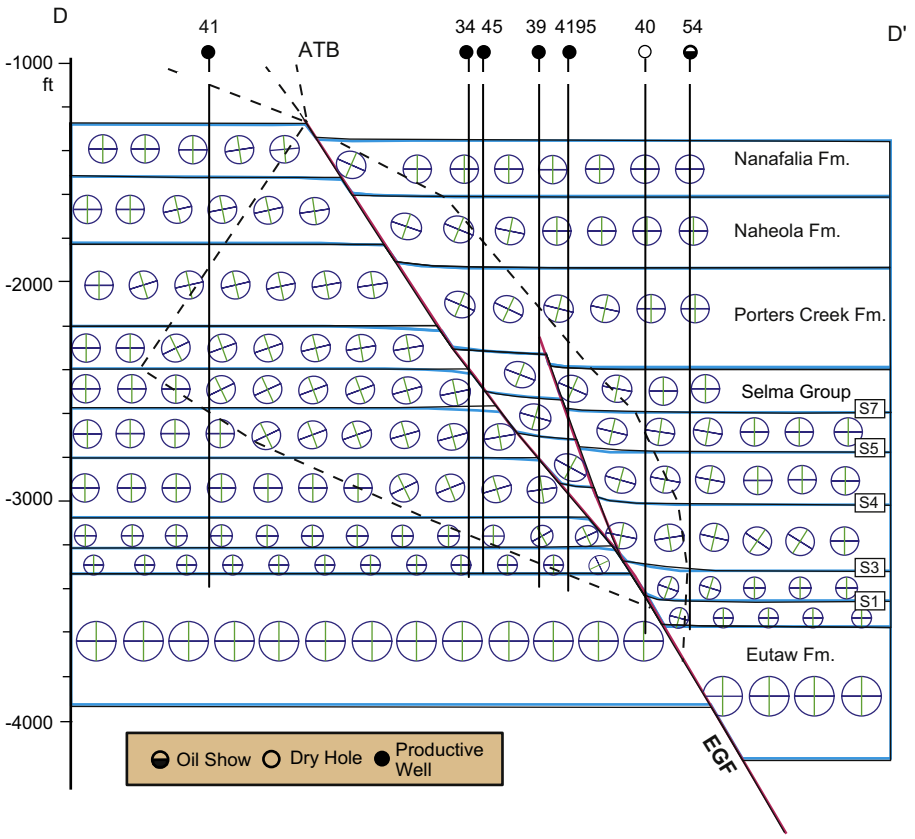

Fig. 13. Cross section D–D′ (thin black lines) overlapped with the trishear predicted extensional fault-propagation fold (thick light lines). Strain ellipses are shown with two principal axes. The growth trishear boundaries in the hanging wall and the footwall are shown as the dashed curves. EGF = East Gilbertown fault, ATB = active trishear boundary.

the sequential evolution of the extensional fault-propagation fold associated with an upward propagating fault predicted by the growth trishear model with compaction. In this model, the fault tip propagates at a dip of 60° throughout the deformation and the change of the fault dip during the subsequent deposition of the units is entirely caused by the compaction of these units. Thus the fault progressively flattens during deformation of the compacted units, and the dip of the fault tip is kept at 60°. The initial stage of the model is similar to the one discussed previously in the non-compaction model. The velocity field and the apical angle are also the same as in the non-compaction model. Because the thickness of each bed when it is deposited is the uncompacted thickness and is thus greater than that in the previous model, the p/s ratios here at each stage are systematically greater those in the previous model.

The results show a remarkable similarity between the final model (Fig. 14g) and the cross section (Fig. 10). The extensional fault-propagation fold is well developed in the hanging wall, and the greatest dips occur in the lower part of the Selma Group close to the fault, which is in accordance with the dipmeter data (Fig. 5). The fold is an upward widening structure as predicted by the trishear model. The fault flattens most in subunits 1 through 3 because they are compacted the most. The fault increases in dip as the units become stratigraphically younger and are less compacted.

The model also has some differences from the uncompacted model. There is an extra dip domain in the hanging wall in Fig. 14g where the Selma chalk is juxtaposed with the Eutaw Formation (bounded by two dashed vertical lines). It is caused by differential compaction between the Eutaw Formation and the Selma Group. In the model, the Eutaw Formation is treated as a non-compactable unit for maximum effect, thus the dips are caused entirely by the compaction of the Selma Group. Also, the compacted strata flatten out upsection due to the decreasing amount of compaction. Another difference between the extensional fault-propagation folds predicted by the compaction and non-compaction growth trishear models is revealed in the bedding dips in the footwall. Bedding in the footwall predicted by the compaction trishear model is much flatter than that predicted by the model without compaction and thus is a better match to the original extensional fault-propagation fold.

6. Conclusions

The geometry of an extensional fault-propagation fold developed above a propagating fault is largely controlled by the p/s ratio according to the growth trishear model. If the p/s ratio is less than 1.0, the fold widens upward in both the hanging wall and footwall. When the p/s ratio is greater than 1.0, the growth trishear fold narrows upward in both the hanging wall and footwall, because the trishear boundaries are convergent upward to the fault tip line. If the p/s ratio is large enough, the fold may terminate upward in a short distance from the initial fault tip and thus the growth strata are deformed by rigid-block translation. The strains in the extensional fault-propagation fold are more concentrated near the fault tip with a smaller p/s ratio than with a larger p/s ratio.

In the Gilbertown graben system, compaction at the level of the Selma Group without trishear cannot produce the observed fold geometry. If the deformation is accomplished purely by compaction, deformation in the hanging wall is vertical simple shear. The

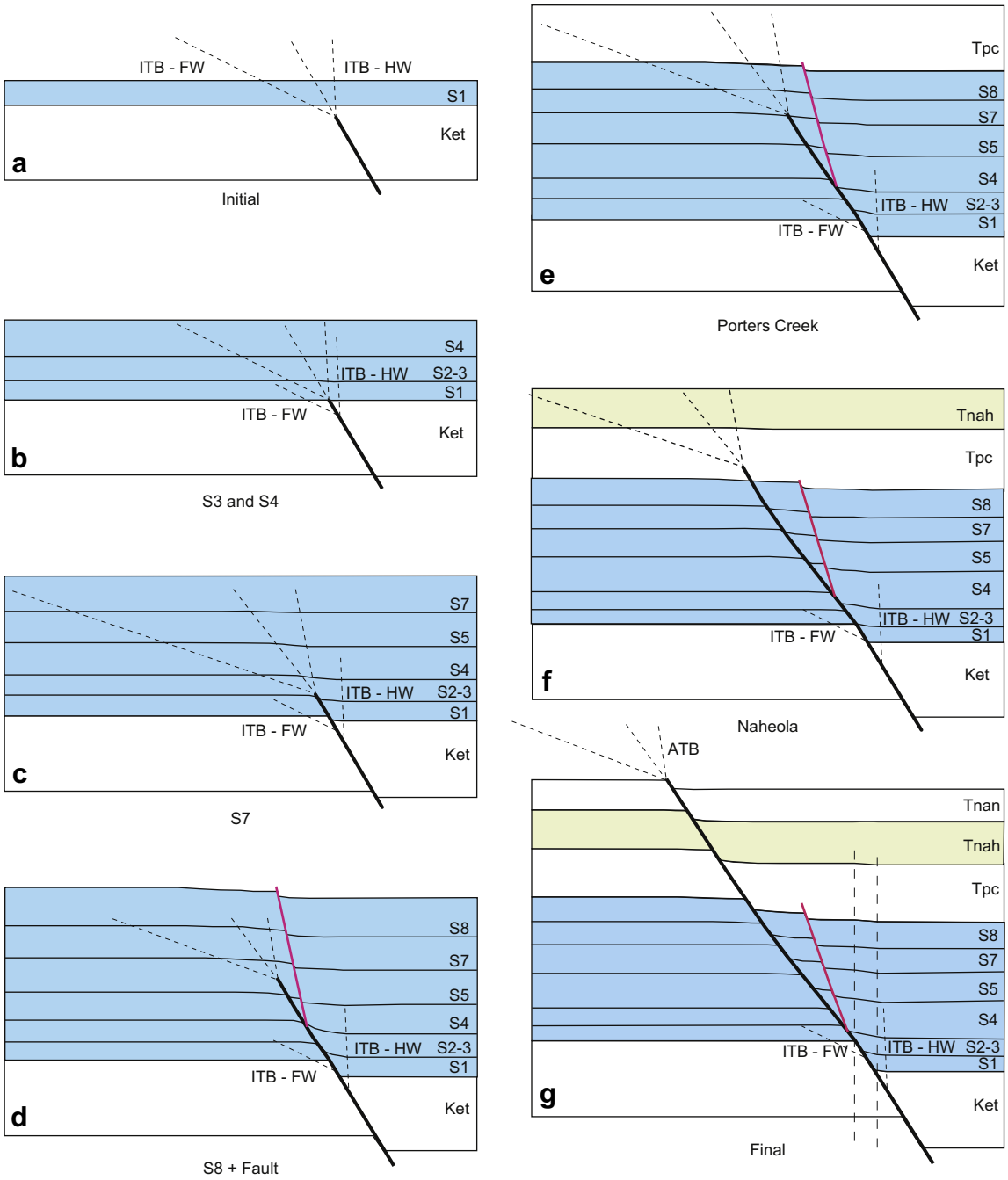

Fig. 14. Sequential forward modeling for cross section D–D′ using trishear model and compaction.

resulting hanging wall fold is a monocline bounded by vertical axial surfaces. The monocline develops right above a fault segment where different rock types are juxtaposed. In the area where the same type of rock is juxtaposed, no fold will form, but the fault is flattened due to the compaction.

The growth trishear model with a component of compaction is the best model to predict the extensional fault-propagation fold in Gilbertown field, although the geometry of the fold can be satisfactorily modeled by both the compaction and non-compaction trishear models. The dip in the footwall predicted by the compaction trishear model is less due to the compaction and is close to the original fold geometry. The strain predicted by the growth trishear model is most significant in the hanging wall close to the master fault.

Acknowledgments

This research was funded by the U.S. Department of Energy under Contract DE-AC22-94PC91008 through BDM-Oklahoma, Incorporated, subcontract G4S51733 and a DOE EPSCoR Grant. We thank John Byrd and Paradigm Geophysical Ltd. for GEOSEC2D and GEOSEC3D software used to construct the 3-D model and cross sections of Gilbertown field. We thank two anonymous reviewers for their constructive and helpful comments of the manuscript.

References

Allmendinger, R.W., 1998. Inverse and forward numerical modeling of trishear fault-propagation folds. Tectonics 17, 640–656.

Athy, L.F., 1930. Density, porosity, and compaction of sedimentary rocks. Bulletin of the American Association of Petroleum Geologists 14, 1–24.
Bengtson, C.A., 1981. Statistical curvature analysis techniques for structural interpretation of dipmeter data. Bulletin of the American Association of Petroleum Geologists 65, 312–332.
Billingsley, L.T., 1982. Geometry and mechanisms of folding related to growth faulting in Nordheim field area (Wilcox), DeWitt county, Texas. Gulf Coast Association of Geological Societies. Transactions 32, 263–274.
Bolin, D.E., Mann, S.D., Burroughs, D., Moore Jr., H.E., Powers, T.J., 1989. Petroleum atlas of Southwestern Alabama, Alabama Geological Survey. Atlas 23, 218.
Braunstein, J., 1953. Fracture-controlled production in Gilbertown field, Alabama. Bulletin of the American Association of Petroleum Geologists 37, 245–249.
Cowie, P.A., Karner, G.D., 1990. Gravity effect of sediment compaction-examples from the North Sea and Rhine Graben. Earth and Planetary Science Letters 99, 141–153.
Current, A.M., 1948. Gilbertown field, Choctaw county, Alabama: Tulsa, Oklahoma. American Association of Petroleum Geologist Structures Typical American Oil Field 3, 1–4.
Davison, I., 1987. Normal fault geometry related to sediment compaction and burial. Journal of Structural Geology 9, 393–401.
Dickinson, G., 1953. Geological aspects of abnormal reservoir pressures in Gulf Coast Louisiana. Bulletin of the American Association of Petroleum Geologists 37, 410–432.
Dula Jr., W.F., 1991. Geometric models of listric normal faults and rollover folds. Bulletin of the American Association of Petroleum Geologists 75, 1609–1625.
Epard, J.L., Groshong Jr., R.H., 1993. Excess area and depth to detachment. Bulletin of the American Association of Petroleum Geologists 77, 1291–1302.
Erslev, E.A., 1991. Trishear fault-propagation folding. Geology 19, 617–620.
Gawthorpe, R.L., Sharp, L., Underhill, J.R., Gupta, S., 1997. Linked sequence stratigraphic and structural evolution of propagating normal faults. Geology 25, 795–798.
Gay Jr., P.S., 1989. Gravitational compaction, a neglected mechanism in structural and stratigraphic studies: new evidence from Mid-Continent. USA. Bulletin of the American Association of Petroleum Geologists 73, 641–657.
Gibbs, A.D., 1983. Balanced cross section construction from seismic sections in areas of extensional tectonics. Journal of Structural Geology 5, 153–160.
Groshong Jr., R.H., 1990. Unique determination of normal fault shape from hanging wall bed geometry in detached half grabens. Eclogae Geologicae Helvetiae 83, 455–471.
Groshong Jr., R.H., 1994. Area balance, depth to detachment, and strain in extension. Tectonics 13, 488–1497.
Groshong Jr., R.H., Pashin, J.C., Chai, B., Schneeflock, R.D., 2003. Predicting reservoir-scale faults with area balance: application to growth stratigraphy. Journal of Structural Geology 25, 1645–1658.
Hamilton, E.L., 1976. Variations of density and porosity with depth in deep sea sediments. Journal of Sedimentary Petrology 46, 280–300.
Hancock, C.J., Scholle, P.A., 1975. Chalk of the North Sea: petroleum and the continental shelf of northwest Europe. Geology 1, 413–427.
Hardy, S., Ford, M., 1997. Numerical modeling of trishear fault-propagation folding and associated growth strata. Tectonics 16, 841–854.
Hardy, S., McClay, K., 1999. Kinematic modelling of extensional fault-propagation folding. Journal of Structural Geology 21, 695–702.
Harris, P.M., Dodman, C.A., 1982. Jurassic evaporites of the U.S. Gulf coast: the Smackover-Buckner contact. In: Hanford, C.R. (Ed.), Depositional and Diagenetic Spectra of Evaporites – a Core Work Shop, 3, pp. 174–192.
Houseknecht, D.W., 1987. Assessing the relative important of compaction processes and cementation to reduction of porosity in sandstones. Bulletin of the American Association of Petroleum Geologists 71, 633–642.
Hughes, D.J., 1968. Salt tectonics as related to several smackover fields along the northeast rim of the Gulf of Mexico basin. GCAGS Transactions 18, 320–330.
Jin, G., Groshong Jr., R.H., 2006. Trishear kinematic modeling of extensional fault-propagation folding. Journal of Structural Geology 28, 170–183.
Jin, G., Pashin, J.C., Groshong Jr., R.H., 1998. Well-based 3-D Visualization of Mature Oil Reservoirs Associated with the Gilbertown Graben, Southwest Alabama. American Association of Petroleum Geoligists Annual Convention, Salt Lake City.
Jin, G., Groshong Jr., R.H., Pashin, J.C., 1999. The relationship between extensional fault-propagation fold geometry and fracture production in the Selma chalk, Gilbertown oil fields, southwest Alabama. GCAGS Transactions 49, 148–149.
Labute, G.J., Gretener, P.E., 1969. Differential compaction around a Leduc Reef-Wizard Lake Area, Alberta. Bulletin of Canadian Petroleum Geologists 17, 305–325.
Martin, R.G., 1978. Northern and eastern Gulf of Mexico continental margin stratigraphic and structural Framework. In: Bauma, A.H. (Ed.), Framework, Facies, and Oil-trapping Characteristics of the Upper Continental Margin, vol. 7. American Association of Petroleum Geologists Studies in Geology, pp. 21–42.
Moore, D.B., 1971. Subsurface Geologic Map of Southwest Alabama, Alabama Geological Survey Special Map 99.
Murray Jr., C.E., 1961. Geology of the Atlantic and Gulf Coastal Province of North America. Harper and Brothers, New York, 692 pp.
O'Connor, M.J., Gretener, P.E., 1974. Quantitative modelling of the process of differential compaction. Bulletin of Canadian Petroleum Geologists 22, 241–268.
Pashin, J.C., Raymond, D.E., Kingsberg, A.K., Alabi, G.G., Carroll, R.E., Groshong Jr., R.H., Jin, G., 1998a. Area balance and strain in an extensional fault system: strategies for improved oil recovery in fractured chalk, Gilbertown field, southwest Alabama. U.S. Department of Energy Fossil Energy Subcontract G4S517363 Final Report, 217.
Pashin, J.C., Groshong Jr., R.H., Jin, G., 1998b. Structural modeling of a fractured chalk reservoir: toward revitalizing Gilbertown field, Choctaw county, Alabama. GCAGS Transactions 48, 335–348.
Pashin, J.C., Raymond, E.E., Alabi, G.G., Groshong Jr., R.H., Jin, G., 2000. Revitalizing Gilbertown oil field: characterization of fractured chalk and glauconitic sandstone reservoirs in an extensional fault system. Geological Survey of Alabama Bulletin 168, 1–81.
Perrier, R., Quiblier, J., 1974. Thickness changes in sedimentary layers during compaction history: methods for quantitative evaluation. Bulletin of the American Association of Petroleum Geologists 58, 507–520.
Qi, J., Pashin, J.C., Groshong Jr., R.H., 1998. Structure and evolution of North Choctaw Ridge Field, Alabama, a salt-related footwall uplift along the peripheral fault system, Gulf coast basin. GCAGS Transactions 48, 349–359.
Roux Jr., W.F., 1979. The Development of Growth Fault Structures. American Association of Petroleum Geologists Structural Geology School Course Notes, 33.
Russell, E.E., Ready, D.M., Mancini, E.A., Smith, C.C., 1983. Upper Cretaceous Lithostratigraphy and Biostratigraphy in Northeast Mississippi, Southwest Tennessee and Northwest Alabama, Shelf Chalk and Coastal Clastics, Tuscaloosa, Alabama. Southeastern Section Society of Paleontologists and Mineralogists Guidebook, Geological Survey of Alabama, 72.
Schlische, R.Q., 1995. Geometry and origin of fault-related folds in extensional settings. Bulletin of the American Association of Petroleum Geologists 79, 1661–1678.
Schlumberger, 1989. Log interpretation: principal and applications. Schlumberger Educational Services , 13–19.
Scholle, P.A., 1977. Chalk diagenesis and its relationship to petroleum exploration: oil from chalk a modern miracle. Bulletin of the American Association of Petroleum Geologists 61, 982–1009.
Skuce, A.G., 1996. Forward modeling of compaction above normal faults: an example from the Sirte Basin, Libya, in Modern Developments. In: Buchanan, P.G. (Ed.), Structural Interpretation, Validation, and Modeling. Geological Society Special Publication No. 99, pp. 135–146.
Suppe, J., Chou, T.T., Hook, S.C., 1992. Rates of folding and faulting determined from growth strata. In: McClay, K.R. (Ed.), Thrust Tectonics. Chapman and Hall, New York, pp. 105–121.
Tolson, J.S., Copeland, C.W., Bearden, B.L., 1983. Stratigraphic profiles of Jurassic strata in the western part of the Alabama coastal plain. Alabama Geological Survey Bulletin 122, 425.
White, N.J., Jackson, J.A., McKenzie, D.P., 1986. The relationship between the geometry of normal faults and that of the sedimentary layers in their hanging walls. Journal of Structural Geology 8, 897–909.
Williams, G., Vann, I., 1987. The geometry of listric normal faults and deformation in their hanging walls. Journal of Structural Geology 9, 789–795.
Wilson, J.C., McBride, E.F., 1988. Compaction and porosity evaluation of Pliocene sandstones, Ventura basin, California. Bulletin of the American Association of Petroleum Geologists 72, 664–681.
Wilson, G.V., Kidd, J.T., Shannon, S.W., 1976. Relationships of surface and subsurface faults in Choctaw and Clarke Counties, Alabama. In: Copeland, C.W. (Ed.), Cretacous and Tertiary Faults in Southwestern Alabama: Alabama Geological Society, Fourteenth Annual Field Trip Guidebook, p. 114.
Withjack, M.O., Islam, Q.T., La Pointe, P.R., 1995. Normal faults and their hanging wall deformation: an experimental study. Bulletin of the American Association of Petroleum Geologists 79, 1–18.
Worrall, D.M., Snelson, S., 1989. Evolution of the northern Gulf of Mexico, with emphasis on Cenozoic growth faulting and the role of salt. In: Bally, A.W. (Ed.), The Geology of North America: an Overview. Geological Society of America. The Geology of North America A, Boulder, Colorado, pp. 97–138.
Xiao, H., Suppe, J., 1989. Role of compaction in the listric shape of growth normal faults. Bulletin of the American Association of Petroleum Geologists 73, 777–786.
Xiao, H., Suppe, J., 1992. Origin of rollover. Bulletin of the American Association of Petroleum Geologists 76, 509–529.
Zehnder, A.T., Allmendinger, R.W., 2000. Velocity field for the trishear model. Journal of Structural Geology 22, 1009–1014.